AIAA 80-0796R

Wind Tunnel Demonstration of Aeroelastic Tailoring Applied to Forward Swept Wings

V. C. Sherrer,* T. J. Hertz,* and M. H. Shirk*
Air Force Wright Aeronautical Laboratories, Wright-Patterson Air Force Base, Ohio

The principle of aeroelastic tailoring with advanced composite materials to increase the divergence speed of a forward swept wing has been demonstrated through low-speed wind tunnel tests. The approach was to perform a low-cost, fairly simple wind tunnel test on a variable sweep cantilever wing model. Available analytical methods were shown to accurately predict the divergence speed of both aluminum and composite plate structures in the subsonic speed range. Methods were evaluated for predicting the onset of divergence using subcritical wind-tunnel data. Results of the analyses and tests are presented in this report.

Nomenclature

A = plate planform area
AR = aspect ratio
B = strain gage calibration constant
C_{L_α} = wing lift curve slope
EI = bending stiffness
F_r = wing restoring force
GJ = torsional stiffness
k = wing structural stiffness
L = lift
q, q_D = dynamic pressure, divergence dynamic pressure
S = wing planform area
W = wing plate weight
α = wing root angle of attack
ϵ = strain
θ = flexible wing angle of attack
Λ = sweep angle
λ = taper ratio

Introduction

UNTIL recently, consideration of divergence has essentially eliminated the forward swept wing as an aircraft design option. The static aeroelastic instability of divergence of lifting surfaces is well known. Bisplinghoff[1] presents the classical trend of divergence speed as a function of wing sweep. In the figure taken from Ref. 1 (Fig. 1), he shows the divergence speed for a conventional wing reduces dramatically with moderate forward sweep, but the divergence speed becomes very high with moderate aft sweep.

Bending deformation affects the aeroelastic behavior of swept wings. For a slender wing with aft sweep, bending produces a reduction in the local angle of attack known as wash-out. However, for a slender wing with forward sweep, bending produces an increase in the local angle of attack or wash-in. Wash-in increases the aerodynamic loading and total flexible lift-curve slope of the wing and thus reduces the aeroelastic divergence speed. An approach to the problem of increasing the divergence speed is to reduce the bending deformation and thus the wing wash-in. For the conventional metallic wing under a given aerodynamic loading, the bending deformation is reduced by increasing the wing bending stiffness which normally requires an increase in structural material with an associated increase in weight.

A different approach to increasing divergence speed is possible when advanced composite materials are used in the wing structure. If one looks a little closer at the problem of divergence, only a reduction in wash-in is required, not necessarily an accompanying reduction in bending. Advanced composites such as graphite-epoxy and boron-epoxy have significantly higher specific stiffness and specific strength characteristics than conventional aircraft metals. Additionally, these properties are directional. The directional properties of composites can be oriented to alter the deformation under loading. By orienting the composites in advantageous directions, wash-in of a forward swept wing can be reduced, and hence the divergence speed can be increased. Thus, the advantages of advanced composites are twofold—high specific stiffness and the directional nature of this stiffness. Therefore, to increase divergence speed, significantly less weight would be required for a composite structure than for a conventional metal structure.

The technology to design for a desired aeroelastic response of a lifting surface using advanced filamentary composite materials has been named aeroelastic tailoring. References 2-8 describe the aeroelastic tailoring technology and its applications. Krone[9] applied the aeroelastic tailoring procedure described in Ref. 2 to design for elimination of aeroelastic divergence. He showed that the weight of executive transport and lightweight fighter wings with sweeps from 35 deg aft to 35 deg forward could be significantly reduced using tailored composites. A weight comparison of a metallic wing and a tailored composite wing for a lightweight fighter is presented in Fig. 2 taken from Ref. 9. The figure shows that for increasing forward sweep the weight required in aluminum to provide adequate stiffness increases much faster than the weight required in tailored composites. Weisshaar[10,11] used laminated beam theory and aerodynamic strip theory to predict the static aeroelastic divergence characteristics of swept wings. He showed that, because of elastic coupling between the bending and torsional deformation of the wing box, laminated composites may be used to preclude divergence for a large range of forward sweep angles.

Since the forward swept wing has not been considered a serious design option, there is a scarcity of data on its structural and aeroelastic characteristics. The Flight Dynamics Laboratory (FDL) recognized the need for experimental data that would illustrate the principle of aeroelastic tailoring with composites and its application to divergence of forward swept wings. This paper summarizes the design, analysis, and testing of an aeroelastic model which incorporates variable forward wing sweep. (Reference 12 presents a complete description of the effort.) Four plates of the same planform, one aluminum and three graphite-epoxy composite plates with different laminate orientations, were individually incorporated in the model as the structural

Presented as Paper 80-0796 at the AIAA/ASME/ASCE/AHS 21st Structures, Structural Dynamics and Materials Conference, Seattle, Wash., May 12-14, 1980; received June 12, 1980; revision received May 5, 1981. This paper is declared a work of the U.S. Government and therefore is in the public domain.

*Aerospace Engineer, Structures and Dynamics Division, Flight Dynamics Laboratory. Member AIAA.

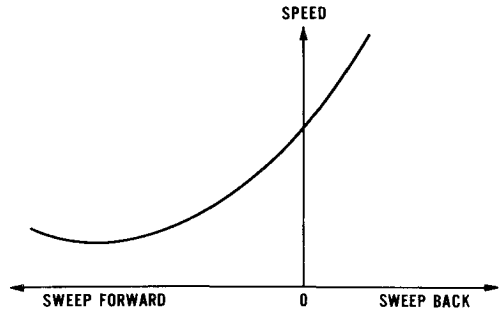

Fig. 1 Variation of divergence speed with sweep (Ref. 1).

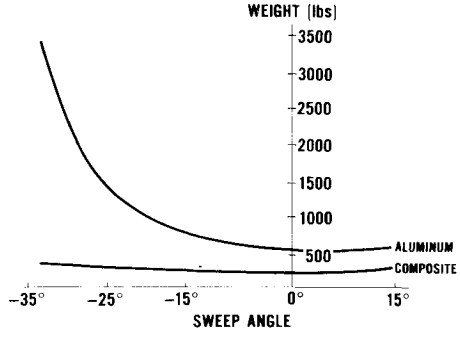

Fig. 2 Lightweight fighter wing skin weight vs sweep (Ref. 9).

element. The test and analysis results illustrate a simple, yet effective, form of aeroelastic tailoring.

Model Design and Fabrication

The wing model design evolved from the basic concept of a cantilevered plate as the load-carrying member within an airfoil-shaped (NACA 0010) polyurethane foam sleeve. The plate concept was required to demonstrate the effect of tailoring of composite materials while allowing divergence of the wing within the available tunnel velocity range. The half-span model was designed to have a removable plate that permitted testing of both aluminum and graphite-epoxy materials while using the same aerodynamic sleeve. The leading-edge sweep of the model could be varied from 0 to 60 deg forward in increments of 15 deg, as shown in Fig. 3. Angle of attack could be varied to obtain subcritical data for divergence projection methods. At −30-deg sweep, the model was designed to diverge at approximately the middle of the velocity range of the Air Force Institute of Technology (AFIT) 5-ft wind tunnel. The maximum velocity of this tunnel is approximately 300 ft/s.

A drawing of the model is presented in Fig. 4. The model was designed with a semispan of 24 in., a full-span aspect ratio of 4, and a taper ratio of 0.4 at −30-deg sweep. A fairing that had been used for a previous test in the AFIT tunnel was adapted for this investigation. The opening in the fairing was minimized by a cover plate for each wing sweep.

With the wing in the 30 deg forward sweep position, as shown in Fig. 4, the leading edge of the plate lies along the 15% chord line. The structural plate root was clamped between two 0.25-in. steel plates. The wing pivoted about a large bolt located near the center of this mechanism. Nine holes located on an arc centered at the pivot were used to align the wing at the desired sweep. Each plate was instrumented with strain-gage rosettes on the reference line 4 in. outboard of the root. Since only differential voltage readings were required for the subcritical divergence projection methods, the gages were not calibrated.

Four plates, one 2024-T6 aluminum and three Narmco 5208/T300 graphite-epoxy, were designed and fabricated. Each plate could be tested at the five sweep positions, allowing 20 wing configurations. The aluminum plate was

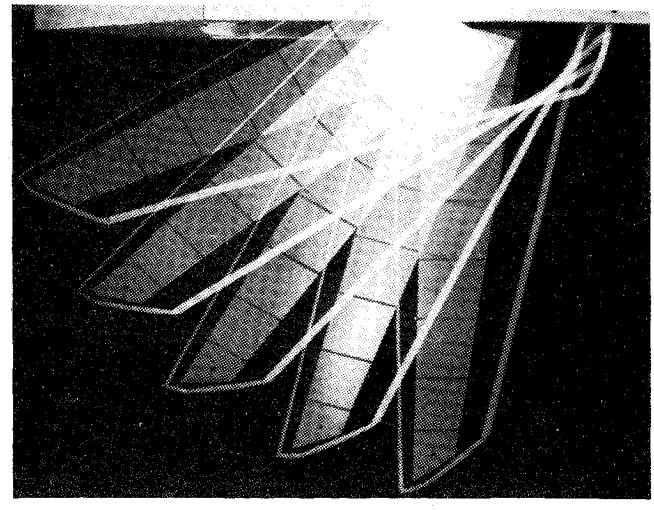

Fig. 3 Five sweep positions of the FDL forward swept wing wind tunnel model.

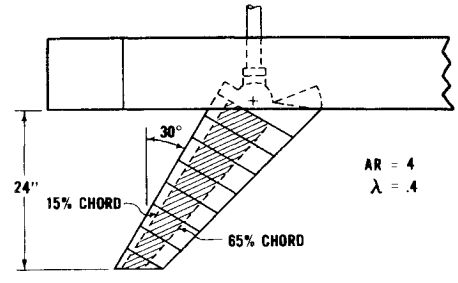

Fig. 4 Schematic of wing model and fairing.

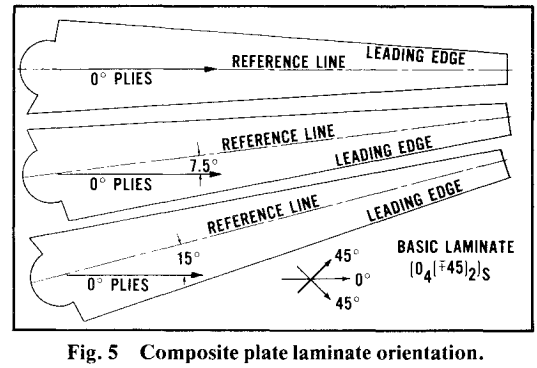

Fig. 5 Composite plate laminate orientation.

0.10 in. thick and the three composite plates consisted of 16 plies of graphite-epoxy with a nominal ply thickness of 5.25 mil. Each of these plates was cut from a larger plate with a symmetric layup, $(0_4,(-45,+45)_2)_S$. Figure 5 shows the orientation of the plate reference line with respect to the 0-deg ply orientation for each of the three composite plates. After curing, the 16-ply laminate had an average total thickness of 0.080 in.

To minimize sleeve stiffness and promote durability, a bridging concept was employed. In the midspan of each section, a ½-in. wide aluminum U-shaped channel was encased in the foam on both sides of the plate. Dowels were added to provide lateral stability to each section and to transmit the airloads on the section into the bridge. After foaming, the sleeve was sectioned to reduce the bending and torsional stiffness contribution. The sections were designed so that only the bridges contacted the plate. Two aluminum bolts, ½ in. from the leading and trailing edges of the plate, fastened each section to the plate. The sleeve mounted on the aluminum plate and the finished composite plates are shown in Fig. 6.

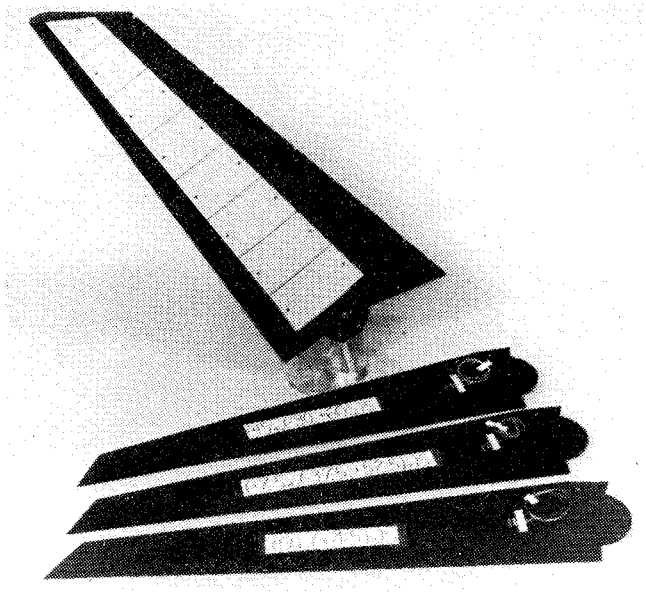

Fig. 6 Wing model with graphite-epoxy plates.

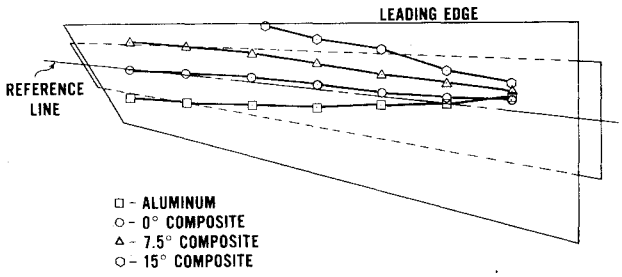

Fig. 7 Zero-twist axes locations.

The elastic properties of the graphite-epoxy were established through coupon tensile testing. The bending and torsional stiffness of the aluminum and composite plates were measured along the reference axis by load deflection tests. With the sleeve section mounted on each of the plates, identical load deflection testing was performed. Results of these tests were used to select the final sleeve design. These data were also used to adjust the math models used to calculate divergence and flutter speeds. The mass, center of gravity, and moment of inertia of each sleeve section were measured and used with calculated mass properties of the plates to establish the total model mass characteristics.

The approximate location of a zero-twist axis was determined for each model configuration. By applying a perpendicular point load on the plate at successive locations between two adjacent sections and observing the twist of the inboard section, a point on this line was found where no twist was observed. Figure 7 shows the zero-twist axis for each of the four models. The aluminum plate model was found to have a zero-twist axis nearly perpendicular to the cantilevered root line. On the composite plates, the location of the zero-twist axis shifted forward with laminate rotation.

Ground vibration tests were conducted on the assembled models for each plate configuration. Figure 8 presents the vibration mode shapes and frequency for the first three modes of the 7.5 deg rotated laminate plate model. Six modes were measured for each model. These data were also used to adjust the math models.

Analysis Methods

Slender beam theory[1] and the method developed by Weisshaar[10] were used to perform preliminary analyses of all the configurations to insure that divergence data could be obtained within the speed range of the wind tunnel. The

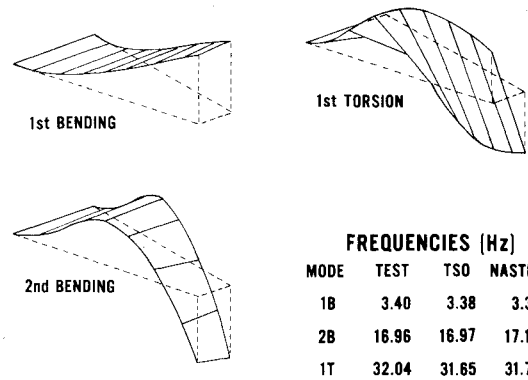

FREQUENCIES (Hz)

MODE	TEST	TSO	NASTRAN
1B	3.40	3.38	3.37
2B	16.96	16.97	17.10
1T	32.04	31.65	31.73

Fig. 8 Mode shapes and frequencies for the 7.5 deg rotated composite model.

analysis was refined using the TSO[2,3] and NASTRAN[15] computer procedures. The TSO and NASTRAN analyses are described below.

TSO Analysis

The aeroelastic tailoring computer procedure TSO is an interdisciplinary preliminary design program combining aerodynamic, static aeroelastic, flutter, and structural calculations. Since low to moderate aspect ratio wings can be modeled as plates, TSO structural analysis is performed using the direct Rayleigh-Ritz energy formulation.

In TSO, a wing structural box is simulated by a trapezoidal plate with depth and skin thickness given by biquadratic polynomials. Three skin orientations may be modeled for a structural box that is symmetric about the midplane. The TSO stiffness polynomial was formulated without regard to stacking sequence, assuming the plies of each orientation are distributed evenly over the skin thickness. For most wing structures, the structural box has a depth much greater than the skin thickness. However, the stacking sequence plays an important role in the overall stiffness of the plate model, since these plates have no core between upper and lower skins. To account for the error induced by the stacking sequence distribution assumed in TSO, equivalent thicknesses were calculated by equating the definition of the flexibility matrix for distributed stacking sequence given in Ref. 2 to the flexibility matrix for a specifically distributed laminate. Then the ply thicknesses for a distributed stacking sequence were calculated to provide the flexibility of the laminate of the desired stacking sequence.

Two computer procedures provide the aerodynamics used in TSO. A steady aerodynamic matrix is calculated by a Woodward aerodynamic routine, ROT.[3,13] This matrix is used with the structural influence matrix generated in TSO to calculate the divergence velocity. An unsteady aerodynamic matrix is provided by a doublet lattice aerodynamic routine, N5KA.[3,14] An aerodynamic matrix is calculated for each of 20 reduced frequencies and a *k*-method modal flutter solution is used to solve for the velocity, frequency, and damping. For a reduced frequency near zero, the corresponding aerodynamic matrix approximates the steady aerodynamic matrix; hence, the divergence velocity can be calculated by the dynamic analysis in TSO.

A sketch of the TSO analysis model is shown in Fig. 9. The trapezoidal structural plate in TSO requires parallel root and tip chords so the analysis model tip was modified as shown. The dashed lines in the sketch represent the airfoil planform. Results from the material properties test and a dimensional check of the finished plate provided the required input data for the plates. The load deflection tests performed on the plates were repeated in the TSO analysis demonstrating a fairly accurate representation of the structural plates. A comparison of the first six measured modal frequencies with those calculated analytically showed that the analytical values

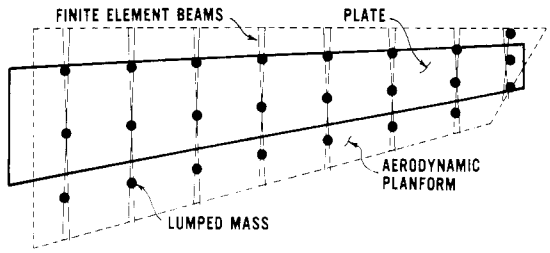

Fig. 9 TSO analysis model.

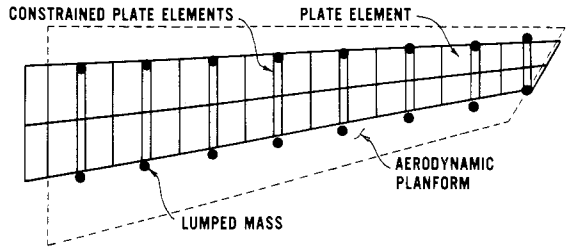

Fig. 10 NASTRAN analysis model.

were too high. Since the analytical model was cantilevered at the root, the lower experimental frequencies were attributed to root flexibility. Therefore, to model the root flexibility, the planform of the plate was slightly altered by extending the plate and moving the root of the analysis model inboard (1 in. for the aluminum plate and 1½ in. for the graphite-epoxy plates). Satisfactory correlation of the natural frequencies was obtained.

Lumped masses and beam elements were used to model the sleeve. Each airfoil section mass was divided into three lumped masses. The locations of the masses are shown relative to the plate in Fig. 9. The beam element feature of TSO was used to account for the stiffness added to the model by the sleeve. This feature allows bending (EI) and torsional (GJ) rigidity constants to model linear spars or ribs. To simplify assigning values of rigidity, it was assumed that the sleeve sections could be modeled by a pair of crossed-beam elements with bending stiffness and no torsional stiffness. The locations are shown in Fig. 9. By iterating the beam element bending stiffness, the first three analytical frequencies were matched to the frequencies of the wind tunnel model. The final analytical and experimental natural frequencies for the 7.5 deg rotated composite model are given in Fig. 8.

Once the pretunnel test data were incorporated in the analysis model, the divergence and flutter calculations were performed. The divergence dynamic pressure predictions for both the static and the dynamic aeroelastic calculations are compared with test data in a later section.

NASTRAN Analysis

The NASTRAN finite-element structural analysis computer program (levels 16 and 17) was used for stress, free vibration, flutter, and divergence analyses. For the aluminum plate, the homogeneous elements CQUAD2 and CTRIA2 were used. For the graphite-epoxy plates, CQUAD1 and CTRIA1 elements were used to simulate the anisotropic properties of the composite laminate. For each of the three composite laminates, representative 3×3 in-plane and bending stiffness matrices were computed and input on MAT2 cards. These stiffness matrices were obtained from program SQ5,[16] which gives the in-plane and bending stiffness of a laminate accounting for ply material properties, ply thickness, stacking sequence, and orientation.

Rigid format 3 of NASTRAN was used to extract the first six normal mode shapes and corresponding frequencies using the inverse power eigenvalue extraction method. The NASTRAN model for the vibration analysis is shown in Fig. 10. The model included the internally calculated plate mass, inertia, and stiffness, the measured mass and inertia characteristics of the sleeve, and the additional stiffness of the sleeve. The mass characteristics of each sleeve section were simulated by a dumbbell mass system. The sleeve sections were modeled by narrow plate elements. The additional torsional stiffness of the sleeve was simulated by rigidly connecting the local chordwise rotational degrees of freedom at the six grid points of these plate elements. As in the TSO simulation, the cantilevered root of the analytical model was set 1.5 in. inboard to compensate for the mount flexibility. The NASTRAN calculated natural frequencies for the 7.5 deg rotated composite model are compared with the TSO and measured values in Fig. 8. Good correlation in frequency and mode shapes was obtained for the four models. Once the vibration models gave satisfactory results, the flutter and divergence calculations were performed.

For the flutter and divergence calculations, rigid format 10 of NASTRAN was used. The rigid format incorporated doublet lattice aerodynamic theory to compute the aerodynamic influence coefficients used in the flutter equation. The k-method of modal flutter solution was used to solve the flutter equation for both flutter and divergence speeds. A range of reduced frequencies, including zero, was used to obtain corresponding values of damping, frequency, and velocity for each of first three normal modes. Flutter of the wing was indicated when the damping of a mode was equal to zero. Divergence of the wing was indicated when the damping and frequency of a mode simultaneously went to zero.

Wind Tunnel Testing

Divergence can be a destructive phenomenon requiring great care in testing. Since 20 wing configurations were to be tested, each with the same foam sleeve, it was necessary to use a testing technique that minimized the likelihood of damage to the model. As will be discussed later, it was possible to obtain "hard," or actual, divergence without serious damage to the model.

The subcritical divergence testing began at 25% of the analytically predicted divergence dynamic pressure. The model angle of attack was varied to measure bending and torsional strains at 1, 2, and 3 deg. Where possible, a minimum of 6 dynamic pressures and strain readings were recorded up to 65% of the projected divergence dynamic pressure. Using the subcritical data, the divergence dynamic pressure was projected by two techniques—a divergence index method developed at the NASA Langley Research Center and a Southwell-type method. As each set of data was obtained, the divergence velocity projections were updated. Only the Southwell-type method is described in this paper.

Southwell's technique[17] was originally developed to project beam buckling by reducing the influence of geometric imperfections. The following is a brief derivation of the techniques for application to divergence.

The lift of a two-dimensional elastic wing section is the sum of the rigid lift due to angle of attack and the incremental lift due to the angle of attack induced by the flexibility:

$$L = qSC_{L_\alpha}(\alpha+\theta) \tag{1}$$

The restoring force of the wing may be written in simple terms as

$$F_r = k\theta \tag{2}$$

and is equal to the lift.

Equating Eq. (1) with Eq. (2) and rearranging terms,

$$\theta = \frac{qSC_{L_\alpha}\alpha}{k - qSC_{L_\alpha}} \tag{3}$$

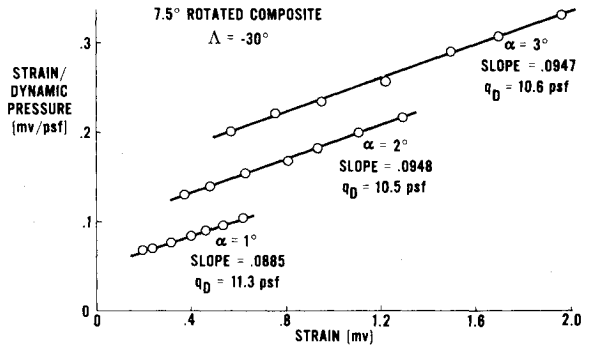

Fig. 11 Southwell-type subcritical divergence projection.

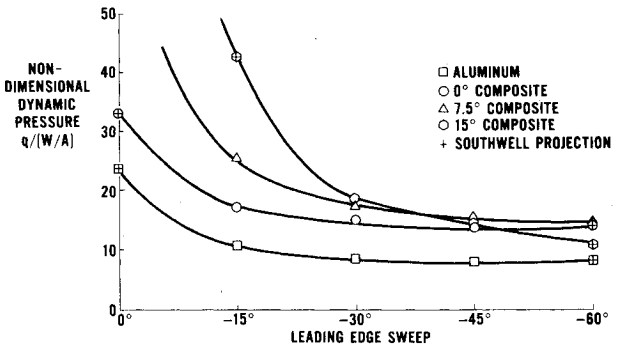

Fig. 12 Nondimensional divergence dynamic pressures vs sweep.

At divergence the denominator of Eq. (3) is equal to zero, producing an infinite θ. Thus the restoring force is just equal to the flexible lift, giving

$$k = q_D S C_{L_\alpha} \tag{4}$$

and thus

$$q_D = \frac{k}{S C_{L_\alpha}} \tag{5}$$

Substituting Eq. (4) into Eq. (3) and solving for the angle of attack as a function of the incremental angle of attack induced by the wing flexibility results in

$$\alpha = \left(\frac{q_D}{q} - 1\right)\theta \tag{6}$$

Measuring strain in a wind tunnel model with a strain gage located near the root provides an indication of the wing deflection due to the flexible lift. The relation of strain to flexible angle of attack is

$$\theta = B\epsilon \tag{7}$$

Substituting Eq. (7) into Eq. (6) results in

$$\alpha = \left(\frac{q_D}{q} - 1\right)B\epsilon \tag{8}$$

or rewriting

$$\frac{\epsilon}{q} = \frac{1}{q_D B}(\alpha + B\epsilon) \tag{9}$$

For use in divergence testing, the deflection, given by a strain measurement at constant angle of attack, is plotted vs the deflection divided by the dynamic pressure. For constant

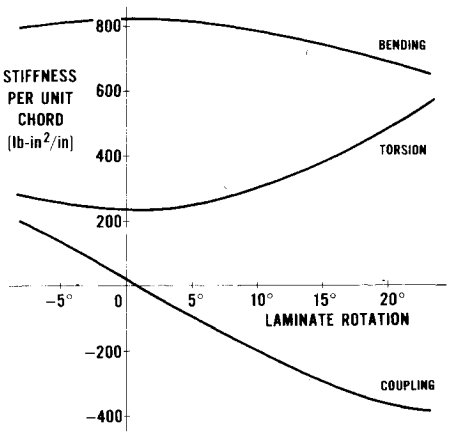

Fig. 13 Stiffness variation for 0 ±45 deg laminates.

angle of attack, the slope of the ϵ/q vs ϵ curve is

$$\frac{d(\epsilon/q)}{d\epsilon} = 1/q_D \tag{10}$$

Hence, the curve is linear and is the inverse of the divergence dynamic pressure.

For each dynamic pressure, strain data are measured and plotted for constant angle of attack. Three sets of data for the 7.5 deg rotated composite model, one for each angle of attack, are presented in Fig. 11. Subcritical projections of divergence dynamic pressures are compared with "hard" divergence points later.

After the subcritical testing was completed on the 20 configurations, the aluminum plate model at −30-deg sweep was selected to obtain a "hard" divergence data point. The Southwell-type subcritical divergence projection technique was used at dynamic pressures up to 65% of divergence. Then, the angle of attack was adjusted to zero and fixed for the remainder of the run. The velocity of the tunnel was raised incrementally until the divergence of the wing occurred, at which time the wind tunnel was immediately shut down.

Fortunately, divergence did not cause damage to the models. The sleeve sections served as a safety device by adding stiffness to the model when the sponge spacers between the sections compressed at large deflections. Thus, the model deflection was limited at divergence. This characteristic of the model made it possible to find the actual divergence points for most of the wing configurations. Several repeated cases demonstrated that the model gave consistent divergence results. The models were not tested to divergence at the −60-deg sweep position because of the greater possibility of sleeve damage. Similarly, no divergence points were obtained at 0-deg sweep because of the possibility of encountering a high-frequency (~25 Hz) flutter instability.

Discussion of Results and Analysis Correlation

Figure 12 shows a comparison of the four model-divergence dynamic pressure boundaries. Two observations concerning the use of a composite material in place of aluminum can be made from this comparison. One is that for all sweeps the composite plates are more effective per unit weight than the aluminum plate in preventing divergence. The second observation is that the divergence speed of the model could be altered by simply rotating the composite plate plies in relation to the reference line of the wing. This effect is especially evident at sweep angles less than −20 deg, where rotation of the composite laminate has the greatest effect.

Rotating the laminate is a form of aeroelastic tailoring. The effect of laminate rotation may be further appreciated by studying Fig. 13, which presents the laminate bending, torsional, and coupling stiffness for each of the composite plates as defined by the method of Ref. 10. Torsional stiffness is

nearly constant between ±5 deg rotation and increases sharply at higher rotation angles. At 15 deg rotation, torsional stiffness is about 60% higher than at 0 deg rotation. The coupling stiffness has a nearly constant slope, increasing negatively from 0 to 15 deg rotation. Negative coupling stiffness produces a wash-out, bend-twist characteristic. At the low forward sweeps, the divergence mode is primarily a torsion mode. Therefore, the increasing torsional and coupling stiffnesses due to the 15 deg rotation have the greatest effect countering the wash-in tendencies and increasing the divergence speed.

Figure 12 shows that the 15 deg rotated composite model has the lowest divergence dynamic pressure of the three composite models at −60-deg sweep. At −45 deg, the 15 deg rotated composite model has a divergence dynamic pressure that is less than the 7.5 deg rotated model. At the greater forward sweeps, the divergence mode is primarily bending and bending stiffness becomes predominate in determining divergence dynamic pressure. The bending stiffness is nearly constant over the ±5 deg rotation range but, at 15 deg rotation, the bending stiffness is about 11% less than that for the nonrotated laminate. Although the coupling and torsional stiffnesses are greatest for this laminate, the bending stiffness is lowest resulting in low divergence speeds at the greater forward sweeps.

Figure 14 presents the "hard" divergence points compared with the subcritical projections based on the Southwell method for the 7.5 deg rotated composite model. Similar results were obtained for the other models. The Southwell method projected divergence dynamic pressures within 10% for the configurations where subcritical data were obtained at test points greater than 50% of the divergence dynamic pressure. It was not possible to obtain data at 50% of the divergence dynamic pressures for the 0-deg sweep cases. Therefore, the quality of convergence of the projections was poor.

Comparisons of the analysis results and test data are presented in Fig. 15. As seen in Fig. 15a for the aluminum model, the divergence dynamic pressure decreases rapidly when the wing is swept from 0 to −15 deg and remains nearly constant from −30 to −60-deg sweep. This trend is predicted very well by TSO and NASTRAN analyses. The TSO and NASTRAN analyses using doublet lattice aerodynamics are in close agreement with the experimental data. The TSO analysis with Woodward aerodynamics consistently predicts slightly higher divergence dynamic pressures than the TSO and NASTRAN analyses with doublet lattice aerodynamics.

The analysis and test divergence data for the nonrotated composite model are presented in Fig. 15b. For the 0-deg sweep case, the flutter dynamic pressure was lower than the divergence dynamic pressure; consequently, testing was restricted to below 35% of the divergence dynamic pressure. This resulted in subcritical projections of divergence dynamic pressure that were not well converged. The correlation be-

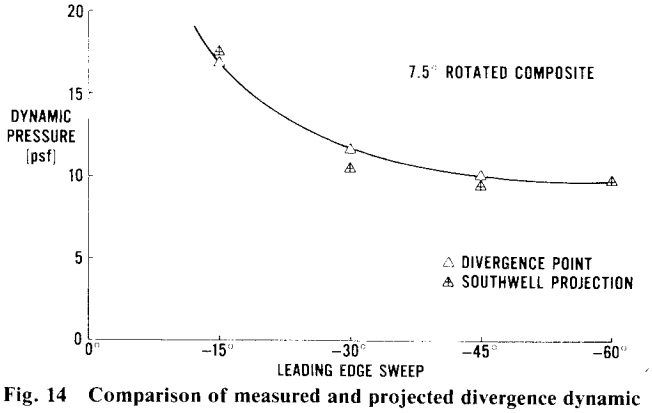

Fig. 14 Comparison of measured and projected divergence dynamic pressures.

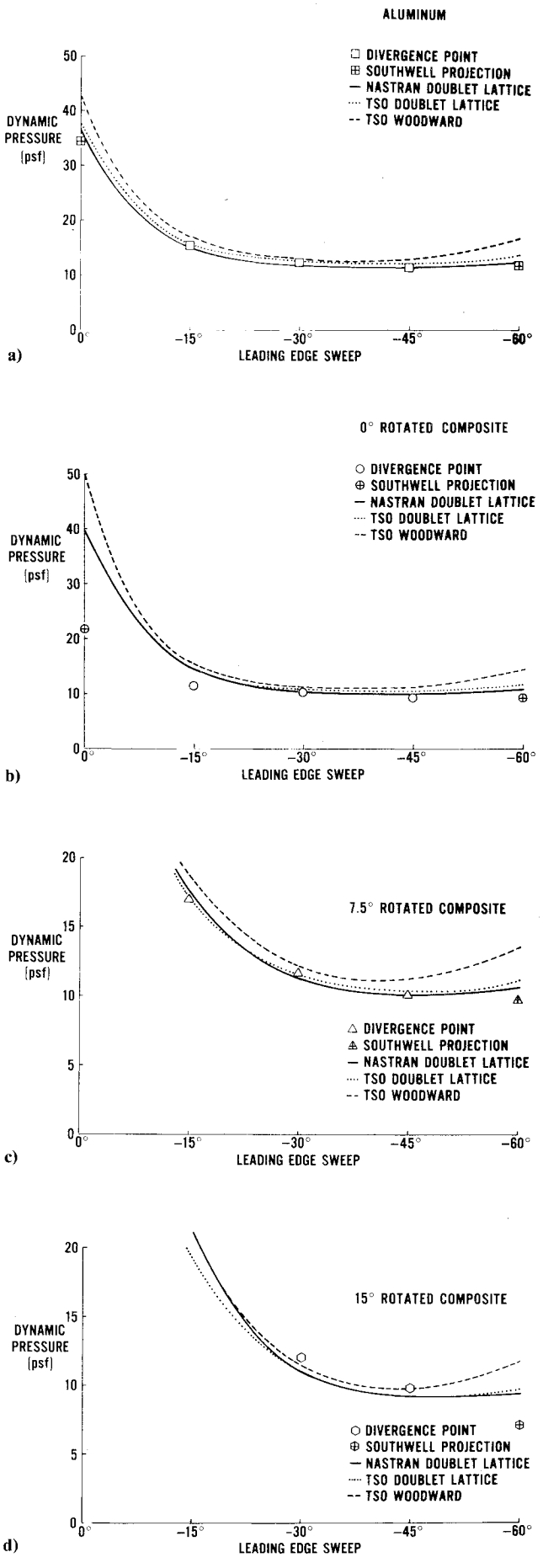

Fig. 15 Comparison of analysis and test divergence dynamic pressures.

Table 1 Divergence dynamic pressures, psf

	Sweep, deg	Test "Hard" point	Southwell	NASTRAN Doublet lattice	TSO Doublet lattice	Woodward
Aluminum	0	—	34.4	36.6	37.4	42.3
	−15	15.5	15.9	15.3	15.8	16.9
	−30	12.3	11.3	11.7	12.6	13.1
	−45	11.5	10.4	11.3	12.1	13.1
	−60	—	11.9	12.4	13.8	16.6
0-deg rotated composite	0	—	21.7	39.6	39.7	49.6
	−15	11.4	11.2	14.4	14.2	15.3
	−30	10.1	8.5	10.6	11.0	11.4
	−45	9.2	8.5	10.0	10.4	11.2
	−60	—	9.3	10.9	11.7	14.1
7.5-deg rotated composite	0	—	116.1	93.2	82.6	203.8
	−15	16.9	17.6	17.8	17.4	18.7
	−30	11.7	10.5	11.3	11.6	12.1
	−45	10.1	9.5	10.1	10.3	11.2
	−60	—	9.8	10.6	11.2	13.5
15-deg rotated composite	0	—	∞	185.4	∞	1407.5
	−15	—	29.3	21.2	19.2	20.9
	−30	12.1	10.9	11.1	11.1	11.5
	−45	9.8	8.9	9.3	9.3	10.1
	−60	—	7.2	9.4	9.8	11.8

tween test and analysis divergence dynamic pressure at −15-deg sweep is poor. This poor correlation caused concern; thus, vibration and load-deflection tests were performed after the wind tunnel tests. Results of these tests indicated a significant reduction in torsional stiffness in the model compared with data obtained prior to the wind tunnel tests. Although not fully explained, it is thought that the violent divergence testing loosened the attachment of the sleeve to the plate reducing the sleeve's contribution to the total model torsional stiffness.

Figure 15c presents the analysis and test divergence data for the 7.5 deg rotated composite model. Rotation of the laminate 7.5 deg forward of the reference line significantly increases the divergence dynamic pressure at 0-deg sweep. As was the case for the nonrotated composite model at this sweep, the Southwell divergence projection was not well converged. The calculated divergence dynamic pressure at 0-deg sweep for the 7.5 deg rotated composite model was at least four times the divergence dynamic pressure for the nonrotated model (Table 1). The NASTRAN and TSO doublet lattice analysis results compare very well with test data for this model at sweeps greater than 15 deg forward. The TSO-Woodward analysis results are consistently higher than the test data.

Figure 15c presents the analysis and test divergence data for the 15 deg rotated composite model. As seen in this figure and in Table 1, the analytical divergence dynamic pressure is very high at 0-deg sweep. It was not possible to obtain a divergence projection at 0-deg sweep using the subcritical techniques. At −15-deg sweep, divergence was very difficult, if not impossible, to define. An unusual phenomenon occurred at approximately the predicted analytical divergence speed. A low-frequency (0.5 Hz) sinusoidal oscillation of the wing began at a low amplitude, and as the dynamic pressure increased, the amplitude of the oscillation increased while the frequency remained constant. The cause of the phenomenon and its mechanism are not understood. It is not predicted by any of the analysis methods and thus may be associated with a characteristic of the model tested. Thus, a meaningful comparison between analysis and test is not possible. At −30 and −45-deg sweep, comparison of test and analysis results is good. However, the −60-deg sweep comparison is not as good. The Southwell projection is 12.4% less than the lowest analytical predictions. Also, the trend of analytical divergence dynamic pressure with sweeps greater than 45 deg forward is opposite to the test results.

The divergence characteristics varied with sweep angle and structural plate. Generally, the severity of divergence, described as the rate of change of deflection as the wing

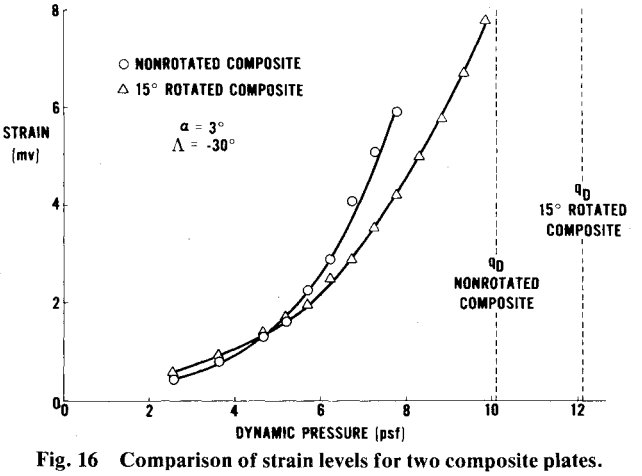

Fig. 16 Comparison of strain levels for two composite plates.

diverged, was greater at the higher forward sweep angles. Rotating the composite laminate forward lessened the severity of the divergence at all forward sweep angles where "hard" divergence points were obtained. At −15-deg sweep, the rate of deformation associated with divergence was mild, while at −45-deg sweep, the rate was rapid. The rapid rate of deformation caused the sleeve sections to compress as a spring which resulted in a postdivergence oscillation (~7 Hz).

At −60-deg sweep, the test results are consistently lower than all of the analysis results for all models. Previous testing involving the fairing revealed that turbulence was generated around the cavity of the fairing. For this present test, cover plates were used to minimize the cavity and reduce the turbulence. The size of the cavity was largest at −60-deg. The turbulence generated by the fairing cavity could have affected the aerodynamic loading on the inboard aft portion of the model. Thus, the center of pressure would be more forward. Since the analysis does not account for the turbulence near the fairing, the calculated center of pressure would be further aft than the actual location on the model. For −60-deg sweep, the effect of cavity turbulence would be greatest, possibly explaining the difference between test and analysis.

The effect of laminate rotation on loading is illustrated in Fig. 16. Measured strain is plotted against dynamic pressure for the nonrotated and 15 deg rotated composite models for −30-deg sweep and at 3 deg angle of attack. For dynamic pressures greater than 50% of the divergence dynamic

pressure of the nonrotated composite model, the strain level is lower for the 15 deg rotated model than for the nonrotated model. Therefore, increasing the divergence dynamic pressure by laminate rotation decreased the level of strain under aerodynamic loading.

Conclusions

Analyses, laboratory tests, and wind tunnel tests of a rather simple, variable sweep model of aluminum and graphite-epoxy composite materials have illustrated the structural design technology of aeroelastic tailoring. The high stiffness-to-weight ratio of the graphite-epoxy is more efficient than aluminum in providing the stiffness required to increase the divergence dynamic pressure. The ability to tailor the composite material for bend-twist coupling significantly adds to the efficiency from a weight standpoint.

Rotating a 0 ± 45-deg composite laminate forward significantly increases the divergence dynamic pressure at leading-edge sweep angles to about -20-deg. A smaller increase in divergence dynamic pressure occurs at -30 and -45-deg sweep. A reversal in the trend occurs at -60-deg.

The analysis methods used predict the divergence dynamic pressures within 5% for all configurations at -30 and -45 deg. For the -15-deg sweep cases of aluminum and 7.5 deg rotated composite, the correlation between analysis results and tests is also within 5%. The analysis of the nonrotated model at -15-deg sweep predicts a divergence dynamic pressure approximately 27% higher than measured. Although not fully explained, the difference between analyses and test of the nonrotated model may have been due to diverging the model several times. Apparently, the large deflections associated with divergence caused a reduction in torsional stiffness probably due to loosening of the aerodynamic sleeve.

The analysis results were consistently higher than the measured values at -60-deg sweep, apparently associated with turbulence from the fairing cavity. Woodward and doublet lattice aerodynamics in static and dynamic analysis methods, respectively, were accurate at sweep angles of -15 through -45 deg. The Woodward static analysis is least accurate at -60-deg sweep predicting higher dynamic pressure than measured.

Rotating the laminate forward does not significantly increase the divergence dynamic pressure at -30-deg sweep. However, the load level at a given angle of attack is significantly reduced at dynamic pressures greater than 50% of the divergence dynamic pressure of the nonrotated laminate.

The subcritical projection methods described accurately project divergence using data obtained at dynamic pressures above 50% of divergence. It may be possible to use similar methods in flight divergence testing.

The rate of change of deflection at the divergence point increases as the wing is swept forward. Rotating the laminate forward decreases the rate of deflection.

Acknowledgments

The assistance of the Air Force Institute of Technology in the fabrication of parts of the divergence model and wind tunnel testing of the model is sincerely appreciated. Special thanks to J. Tiffany, R. Ruley, and R. Murry of the AFIT model shop, and S. Whitt and N. Yardich at the AFIT 5-ft wind tunnel. Thanks also goes to R. Achard and his staff in the FDL Composites Facility Group for their help in constructing the composite plates. Appreciation is also extended to L. Wilson and M. Lipik for their diligent work in preparation of the manuscript and visual aids.

References

[1] Bisplinghoff, R. L., Ashley, H., and Halfman, R. L., *Aeroelasticity,* Addison-Wesley Publishing Company, Inc., Reading, Mass., 1955, pp. 421-526.

[2] McCullers, L. A. and Lynch, R. W., "Dynamic Characteristics of Advanced Filamentary Composite Structures," Vols. I-III, AFFDL-TR-73-111, Sept. 1974.

[3] Lynch, R. W., Rogers, W. A., and Braymen, W. W., "Aeroelastic Tailoring of Advanced Composite Structures for Military Aircraft," Vols. I-III, AFFDL-TR-76-100, Feb. 1978.

[4] Shirk, M. H. and Griffin, K. E., "The Role of Aeroelasticity in Aircraft Design with Advanced Filamentary Composite Materials," *Proceedings of the Second Conference on Fibrous Composites in Flight Vehicles,* Dayton, Ohio, May 1974, pp. 405-437.

[5] Austin, F., Hadcock, R., Hutchings, D., Sharp, D., Tang, S., and Waters, C., "Aeroelastic Tailoring of Advanced Composite Lifting Surfaces in Preliminary Design," *Proceedings of the AIAA/ASME/SAE 17th Structures, Structural Dynamics, and Materials Conference,* Valley Forge, Pa., May 1976.

[6] Lerner, E. and Markowitz, J., "An Efficient Structural Resizing Procedure for Meeting Static Aeroelastic Design Objectives," AIAA Paper 78-471, April 1978.

[7] Triplett, W. E., "Aeroelastic Tailoring Studies in Fighter Aircraft Design," AIAA Paper 79-0725, April 1979.

[8] Gimmestad, D., "An Aeroelastic Optimization Procedure for Composite High Aspect Ratio Wings," AIAA Paper 79-0726, April 1979.

[9] Krone Jr., N. J., "Divergence Elimination with Advanced Composites," AIAA Paper 75-1009, Aug. 1975.

[10] Weisshaar, T. A., "Aeroelastic Stability and Performance Characteristics of Aircraft with Advanced Composite Sweptforward Wing Structures," AFFDL-TR-78-116, Sept. 1978.

[11] Weisshaar, T. A., "Forward Swept Wing Static Aeroelasticity," AFFDL-TR-79-3087, June 1979.

[12] Sherrer, V. C., Hertz, T. J., and Shirk, M. H., "A Demonstration of the Principle of Aeroelastic Tailoring Applied to Forward Swept Wings," AFWAL-TR-81-3066, April 1981.

[13] Gustavsson, S. A. L., "A Computer Program for the Prediction of Aerodynamic Characteristics of Wing-Body-Tail Combination at Subsonic and Supersonic Speeds," The Aeronautical Research Institute of Sweden, Rept. FFA AU-635, Pt. 2, Stockholm, Sweden, Nov. 1972.

[14] Giesing, J. P., Kalman, T. P., and Rodden, W. P., "Subsonic Unsteady Aerodynamics for General Application," AFFDL-TR-71-5, Nov. 1971.

[15] *The NASTRAN User's Manual, (Level 17.0),* NASA SP-222(04), Dec. 1979.

[16] Reed, D. L., "Point Stress Laminate Analysis," General Dynamics, Fort Worth Div., Fort Worth, Texas, FZM-5494, April 1970.

[17] Simitses, G. J., *Introduction to the Elastic Stability of Structures,* Prentice Hall, Englewood Clifs, N. J., 1976, pp. 66-68.